Proc. Natl. Acad. Sci. USA
Vol. 82, pp. 785–789, February 1985
Cell Biology

Structure of the signal recognition particle by electron microscopy

(signal recognition particle/electron microscopy of ribonucleoproteins/negative stain/dark-field imaging)

DAVID W. ANDREWS*, PETER WALTER†, AND F. PETER OTTENSMEYER‡

*‡Department of Medical Biophysics, University of Toronto and Ontario Cancer Institute, 500 Sherbourne Street, Toronto, Ontario, Canada M4X 1K9; and †Department of Biochemistry and Biophysics, University of California Medical School, San Francisco, CA 94143

Communicated by Joan A. Steitz, September 25, 1984

ABSTRACT **The signal recognition particle (SRP) is a ribonucleoprotein consisting of six distinct polypeptide components and one molecule of small cytoplasmic RNA (7SL RNA). The particle was previously shown to function in protein translocation across and protein integration into the endoplasmic reticulum membrane. Homogeneous signal recognition particle preparations were visualized by electron microscopy (*i*) after negative staining, (*ii*) by dark-field imaging of unstained specimens, and (*iii*) by platinum-shadowing. The results of each of these different techniques indicate that the signal recognition particle is a rod-shaped particle 5–6 nm wide and 23–24 nm long.**

The signal recognition particle (SRP) is an 11S ribonucleoprotein consisting of six distinct polypeptides (M_r 72,000; 68,000; 54,000; 19,000; 14,000; and 9,000) (1) and one molecule of RNA (300 nucleotides, termed 7SL RNA) (2). SRP was shown to function as the cellular adapter between the cytoplasmid protein-translation apparatus and the membrane-associated protein-translocation machinery of the endoplasmic reticulum (3, 4). By use of a cell-free translation system programmed with specific mRNAs and supplemented with purified SRP and/or microsomal membranes the following sequence of events has been determined: (*i*) Translation of any mRNA begins on free, cytoplasmic ribosomes. (*ii*) If the nascent chain contains a signal sequence that designates the protein as a candidate to be translocated across (secretory or lysosomal proteins) or integrated into (integral membrane proteins) the endoplasmic reticulum membrane, then SRP tightly interacts with the translating ribosome and reversibly arrests protein synthesis (4). (*iii*) This elongation arrest is released only by direct interaction of SRP with the SRP receptor (5, 6), an integral membrane protein of the endoplasmic reticulum, specifying that the correct target membrane has been reached. The functional ribosome–membrane junction is formed and translocation of the nascent polypeptide proceeds by an unknown mechanism.

As described above, SRP is a well characterized, relatively small particle and has been purified to homogeneity. A multiplicity of interactions with other cellular structures has been described (for a recent review on SRP function see ref. 7). For our understanding of the molecular details of these events, extensive structural information on SRP will be required. Here, our first attempts to visualize SRP by a variety of electron microscopic techniques indicate that the particle can be described as an elongated cylinder.

MATERIAL AND METHODS

Isolation of SRP. SRP was salt-extracted from canine pancreatic microsomes and purified by chromatography on aminopentylagarose followed by velocity sedimentation in sucrose gradients as previously described (8, 9). The 11S peak was collected, quick-frozen in liquid nitrogen and stored at −80°C until used. The SRP preparations used in these studies were enzymatically active (9) and >95% pure as judged by analysis on Coomassie blue-stained NaDodSO$_4$/polyacrylamide gels as well as on ethidium bromide-stained urea/polyacrylamide gels (2).

To stabilize SRP activity, we included 0.01% Nikkol (a nonionic detergent: octaethyleneglycol monododecyl ether; Nikko, Tokyo, Japan) in all buffers (1, 9). The detergent was omitted in the final sucrose gradient centrifugation step, to avoid its possible interference in the imaging techniques. Control experiments showed that in negative stain (bright field) and unstained (dark field) preparations the structures observed were indistinguishable whether prepared in the presence or absence of Nikkol.

Specimen Preparation. Specimens were supported on thin carbon films (about 2 nm thick) made by indirect deposition (10). These films were supported by carbon-backed fenestrated cellulose acetobutyrate films on 3-mm, 200-mesh copper microscope grids. SRP, stored at a concentration of 200–350 μg/ml in 12% (wt/vol) sucrose/50 mM triethanolamine·HOAc, pH 7.5/500 mM KOAc/5 mM Mg(OAc)$_2$/1 mM dithiothreitol, was diluted to a concentration of 2–10 μg/ml with 10 mM triethanolamine·HOAc, pH 7.5/1 mM Mg(OAc)$_2$/0.2 mM dithiothreitol. Samples were centrifuged at 10,000 × *g* for 10 min and applied to grids by injection (11) at a final concentration of 1–5 μg/ml. To modulate their adhesive properties, some carbon films were pretreated with 100 mM HOAc (10). After 1 min, specimens were washed with distilled deionized water.

Specimens were negatively stained with 1% (wt/vol) phosphotungstic acid, wicked, and air-dried. Specimens for critical-point drying were applied in the same manner as above to carbon films or to freshly cleaved mica. The substrate subsequently was passed through solutions of increasing ethanol concentrations (steps of 20%) up to 100% ethanol, followed by increasing concentrations of amyl acetate up to 100%. The sample was then dried in a critical-point drying apparatus (Denton Vacuum, Cherry Hill, NJ) above the critical point of CO_2.

Particles critical-point-dried on mica were shadowed by thermal evaporation of Pt/C pellets (Ladd Research Industries, Burlington, VT) at a distance of 11 cm. Specimens were shadowed in the primary direction for 30 sec, rotated 90°, and shadowed for an additional 5–10 sec. The shadowing angle estimated from latex spheres shadowed in a similar fashion was 10 ± 2°. After shadowing, a thin film was evaporated directly onto the mica substrate. The film was floated off onto water, transferred to grids covered with carbon-backed fenestrated plastic, and photographed in tilt-beam dark field for improved contrast.

Electron Microscopy. Micrographs were taken on a Phillips EM 300 electron microscope at 80 kV at nominal magnifica-

The publication costs of this article were defrayed in part by page charge payment. This article must therefore be hereby marked "*advertisement*" in accordance with 18 U.S.C. §1734 solely to indicate this fact.

Abbreviation: SRP, signal recognition particle(s).

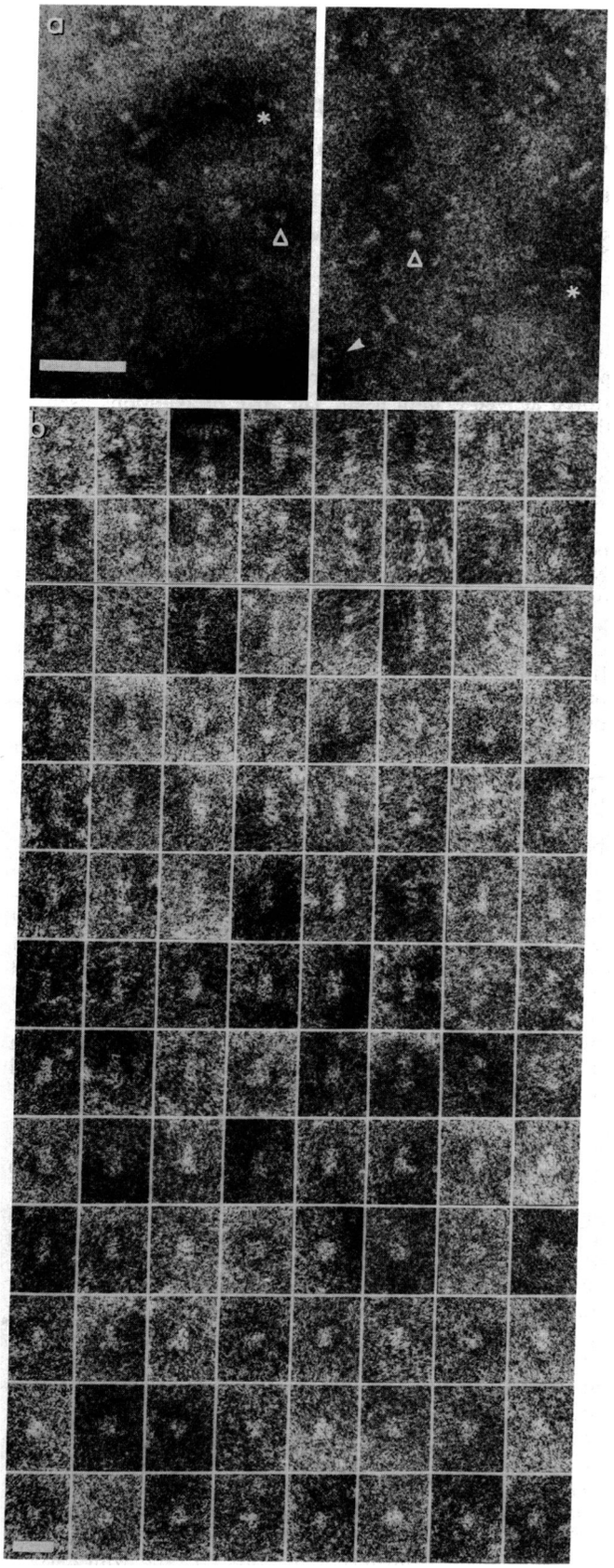

FIG. 1. Bright-field electron micrographs of SRP negatively stained with phosphotungstic acid. (*a*) Large uniformly stained areas. Structures indicated are rod shapes (asterisks), circular structures (triangles), and an aggregate (arrowhead). (Bar = 50 nm.) (*b*) Presentation of 104 of 144 putative molecular images from one micrograph. Arranged with rod shapes at the top and circular structures below. The remaining 40 structures were indistinguishable from those shown. (Bar = 20 nm.)

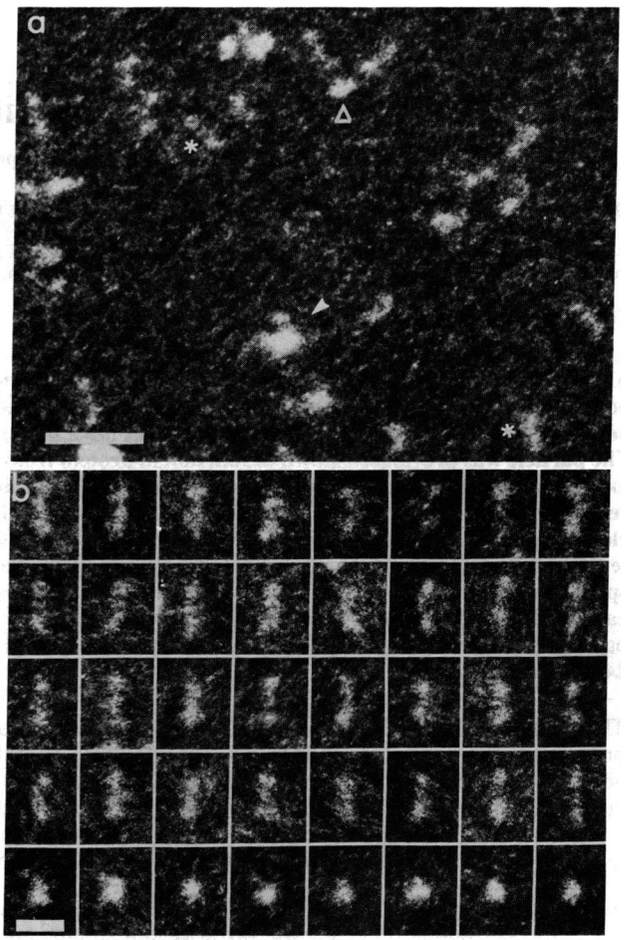

FIG. 2. Dark-field electron micrographs of unstained SRP. (*a*) Overview. Structures indicated are rod shapes (asterisks), a circular structure (triangle), and an aggregate (arrowhead). (Bar = 50 nm.) (*b*) Enlargements of typical structures. Particles spread in the presence or absence of the nonionic detergent Nikkol are intermixed. For comparison, see the first two images in the second row, spread in the presence and absence of Nikkol, respectively. (Bar = 20 nm.)

tions of ×31,000 or ×39,900. Magnification was calibrated using a silicon monoxide grating replica (Fullam, Schenectady, NY). A 500-μm condenser aperture and a 40-μm objective aperture were used (12). Electron Image Plates (Kodak) were exposed to a developed OD of about 0.4 under standard developing conditions for intermediate grain size. Dark-field imaging was accomplished by tilted-beam illumination. To minimize specimen damage minimum beam-exposure techniques were used (13) in addition to the optimum objective aperture and fast-recording plate. With such measures dark-field electron micrographs of unstained macromolecules have been obtained that show higher-resolution detail than possible in bright-field micrographs (12, 14, 15). For the latter, resolution is limited by the necessary heavy-atom stain.

Electron image plates were examined under a low magnification dissecting microscope for optimum focus, lack of astigmatism, and lack of specimen drift. Regions of micrographs of good optical quality, showing a good dispersion of structures larger than 5 × 5 nm and smaller than 30 × 30 nm, were chosen for analysis. Shadow lengths were recorded only for those particles oriented with their long axes normal to the primary shadow direction.

Optical Density Measurements. Dark-field electron micrographs were digitized with a microdensitometer (Perkin–Elmer Model 1010A) from large areas from two micrographs; one area contained 210 structures, and the other, 38 structures. Each picture element corresponded to a 0.5 × 0.5 nm area. The OD was integrated over an area slightly larger than the object (10 × 10 nm, 10 × 25 nm, or 30 × 30 nm) and the average OD of an equivalent area of carbon film was subtracted. A histogram was calculated with bin size of 3.0 OD units and was plotted as a smooth curve by convolution with a spline of length 5.0 OD units, using an interactive display system (Genisco GCT-300, Costa Mesa, CA and Digital Equipment VAX 11-780, Maynard, MA). Integrated OD values were normalized so that the mode value for structures between 10 × 10 nm and 10 × 25 nm equaled one. The gray-level response of the system was calibrated by use of a photographic step tablet (Calibrated No. 2, Kodak).

RESULTS

We have used a variety of different techniques in sample preparation and electron microscopy to examine the structure of SRP. Homogeneous preparations of SRP were imaged negatively stained, by bright-field microscopy (Fig. 1), as well as unstained (Fig. 2) or platinum-shadowed (Fig. 3), by dark-field microscopy. In each case, we observed a predominance of rod-shaped structures with similar widths but various lengths, as well as small circular structures with almost constant diameter. The interpretation of the conformation of SRP consistent with all these images is a cylindrical particle viewed at random orientations (rod-shaped image: lying flat or at an angle, circular image: end-on). To guard against subjective bias in selecting putative SRP images, we included all visible structures falling within a certain size range in our analysis.

The SRP has an estimated M_r of 335,000. Thus, assuming a partial specific volume of 0.73 for protein (16) and 0.53 for RNA (17), the volume of the SRP would be 380 nm^3, which corresponds to a minimum spherical diameter of 9 nm. Based on this calculation, we arbitrarily chose the range 5–30 nm in diameter as a reasonable window to include any SRP images.

A representative area imaged after negative staining is shown in Fig. 1*a*. Rod-shaped or circular structures are indicated by asterisks and triangles, respectively. Representative structures were aligned in the gallery in Fig. 1*b*. Included in this gallery are 104 of the 144 putative SRP images fitting the size criteria from a large uniformly stained area on a single plate. The remaining structures were indistinguishable from those shown and were omitted because of space limitations.

The use of stain to provide contrast can be obviated by imaging unstained SRP in dark field (Fig. 2). In this technique, contrast is dependent only on the particle thickness relative to the carbon support. The structures observed by this technique in the size range of interest are very similar to those obtained with negative stain. In contrast to those results, full-length rod shapes are about 2.5 times more prevalent than circular shapes. This trend might be expected, since there is no stain present to support molecules with oblique orientations during specimen drying. The larger structures seen in the overview in Fig. 2*a* most likely result from aggregation of smaller particles, since they become less frequent when SRP is further diluted. Neither the inclusion

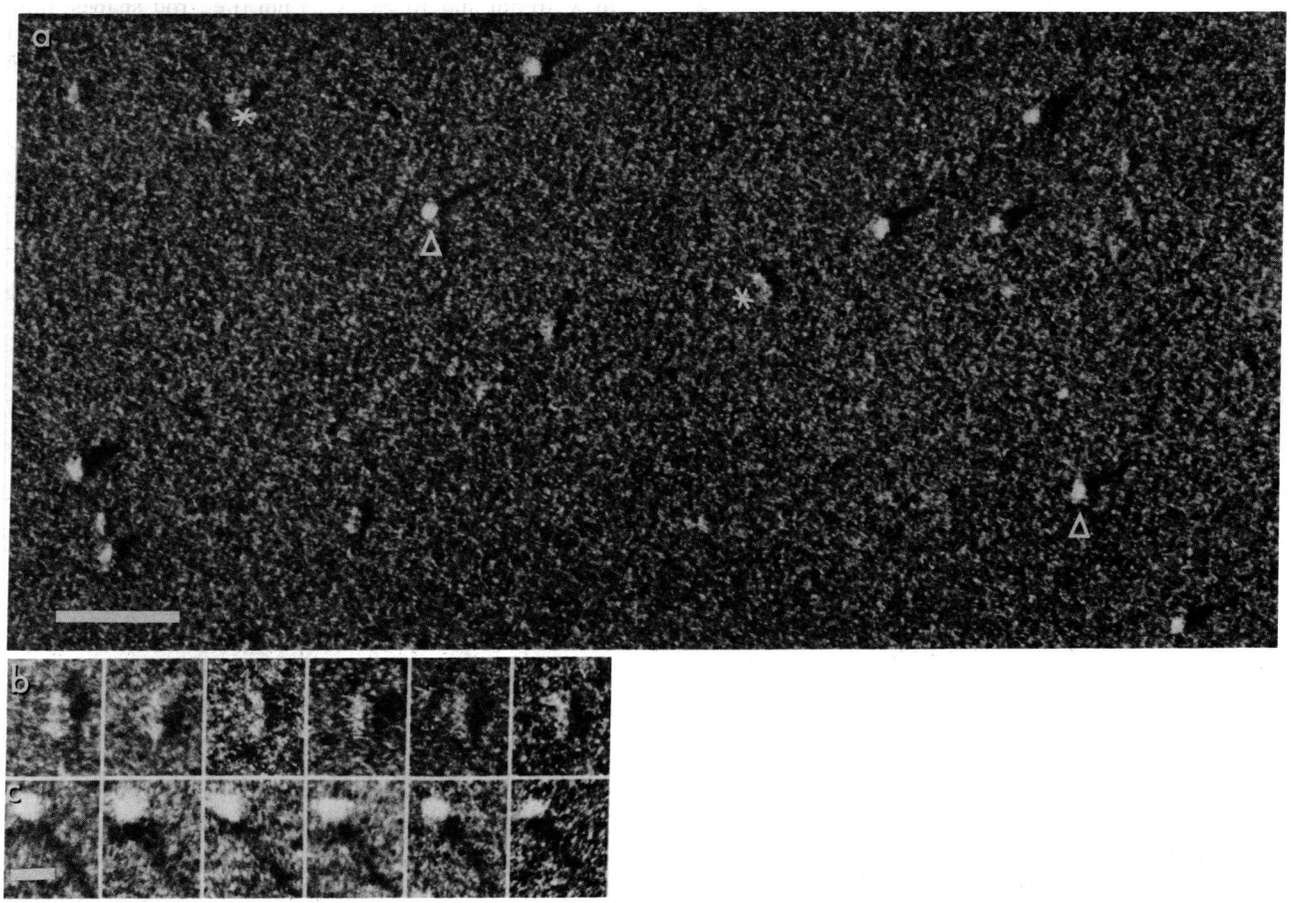

FIG. 3. Dark-field electron micrographs of SRP shadowed with Pt/C. (*a*) Overview. Structures indicated are rod shapes (asterisks), and circular structures (triangles). (Bar = 100 nm.) (*b*) Enlargements of rod shapes. (*c*) Enlargements of circular structures. (Bar = 20 nm.)

of small concentrations of nonionic detergent, nor the application of critical-point drying techniques (designed to minimize structural changes caused by surface tension), nor fixation with gluteraldehyde had any effects on the kinds of structures observed (data not shown).

To confirm that the circular structures are distinct from the rod-shaped ones only by virtue of the angle of immobilization on the support, we platinum-shadowed preparations of critical-point-dried SRP on mica (Fig. 3). Again, except for aggregates, all of the structures are either circular or rod-shaped and are of dimensions similar to those of the structures observed by the techniques described above. The predominant shadow length for the circular structures, a measure of the relative height of the particles, is considerably longer than that measured for the rod shapes.

Fig. 4 is a quantitative analysis of the widths and lengths of structures imaged by negative stain (Fig. 4*d*), dark-field (Fig. 4*c*), and Pt/C shadowing techniques (Fig. 4*b*). It is apparent that with each approach a rather uniform distribution of particle widths is observed: 6.0 ± 0.1 nm for negative stain, 5.6 ± 0.05 nm for dark-field, and about 10 nm for the Pt-shadowing. In each case the longer axis of the particles appears as a continuum ranging from almost circular structures to rod shapes of lengths 23 nm, 24 nm, and 30 nm for negatively stained, dark-field imaged and shadowed SRP, respectively. Because a Pt/C cast is built up around the specimen during shadowing, the dimensions obtained from shadowed images are overestimations of the actual size of the SRP.

The analysis of shadow lengths as a function of particle-image length (Fig. 4*a*) indicated that virtually all elongated structures show a short shadow, consistent with their lying flat on the support. In contrast, circular structures predominantly had shadows about three times longer, albeit a population of circular structures with shorter shadows was also present (see below).

In dark-field imaging the recorded image is generated by electrons scattered by the unstained specimen itself. Since to a first approximation the number of these scattered electrons is proportional to the mass of the sample (18), the relative mass of a given structure can be obtained by integrating the optical density of the photographic image. A curve derived from a histogram of such measurements from dark-field micrographs of SRP is shown in Fig. 5. The solid line represents the integrated optical density of 206 of 210 structures observed. Four structures showed densities beyond the scale of the graph. An apparently uniform distribution of mass is seen with very few values at two times and three times the predominant mass. We arbitrarily dissected this curve into contributions from either all structures between 10 × 10 nm and 10 nm × 25 nm (i.e., rod shapes, dotted curve) or structures smaller than 10 nm across (i.e., circular shapes, dashed curve). A small percentage of structures are

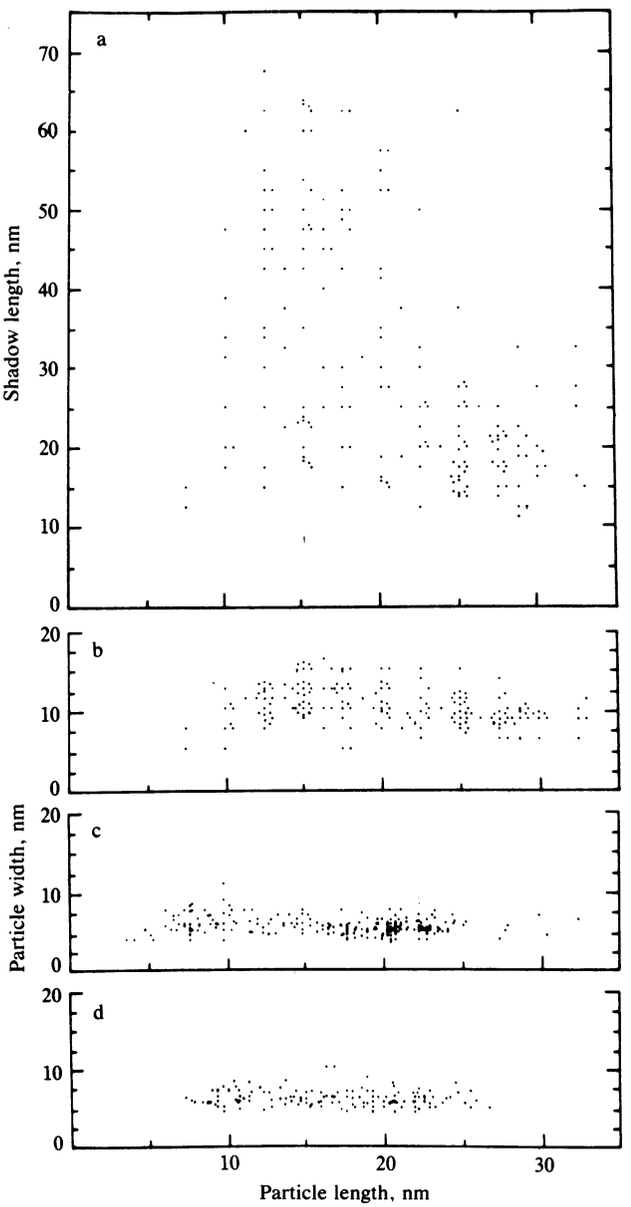

FIG. 4. Measurements from electron micrographs of SRP. (*a*) Shadow length vs. image length for 184 particles shadowed with Pt/C. (*b–d*) Image width vs. image length for the same structures as in *a* (*b*), dark-field electron micrographs of 271 unstained particles (*c*), and bright-field electron micrographs of 144 particles negatively stained with phosphotungstic acid (most of these particles are shown in Fig. 1) (*d*). Each dot represents one particle. Where possible, overlapping points were offset in a circular pattern.

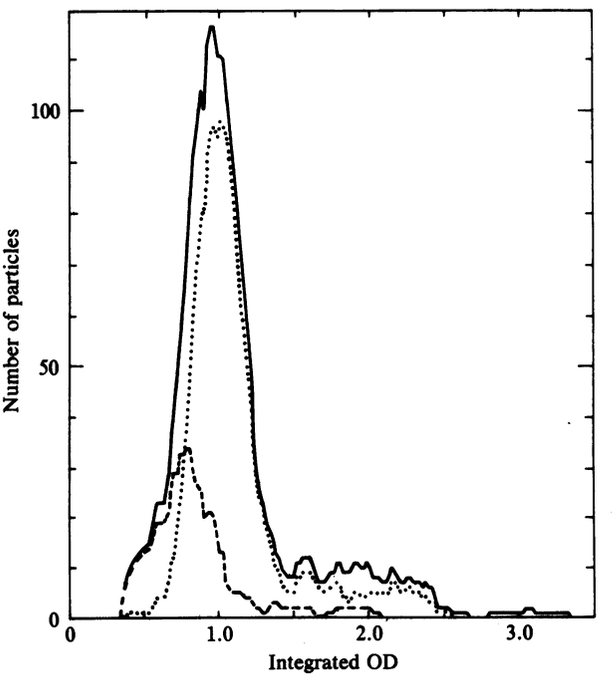

FIG. 5. Curves derived from a histogram of integrated optical densities measured for 210 structures from dark-field electron micrographs of unstained SRP. Solid line, all structures; dotted line, rod-shapes; dashed line, circular structures. Of all structures measured, 72% have an integrated OD within the full width at half maximum of the curve for rod-shapes. Similar curves plotted for SRP spread from buffer not including the detergent Nikkol gave the same profile.

of lower relative mass. These are mostly circular structures and could result from some dissociation of SRP during specimen preparation for microscopy or from increased mass loss of rod-shaped particles oriented in the direction of the electron beam. The first explanation is consistent with the small population of circular structures with short shadows observed in Fig. 4*a*.

DISCUSSION

We have examined the conformation of SRP by three different electron microscopic techniques. During specimen preparation, SRP was exposed to a wide variety of different conditions, including high concentrations of phosphotungstic acid, carbon and mica substrates, air and critical-point drying, and buffers with and without detergent. The spreads of particles obtained from all these variations were very similar. In each case, micrographs showed a series of structures of relatively uniform width (5–6 nm) with a continuous distribution of lengths, from small enough to result in circular images to long enough to imply a 22- to 24-nm-long rod-shaped structure with an axial ratio of about 3.5 imaged by various random orientations. From these dimensions and by assuming a uniform cylinder, we calculate a volume for the SRP of 525 nm^3, which is in good agreement with the 380-nm^3 volume estimated from the SRP's molecular composition. From the images in Figs. 1–3, it is apparent that the SRP is not a uniform cylinder. Various indentations and crevices are seen in the structure, which appear to divide the SRP into three domains along its main axis and effect a structure of lower volume.

The knowledge about the molecular dimensions of SRP has considerably influenced our view of how the particle could functionally interact with the protein-translation machinery. SRP recognizes the information contained in signal sequences of nascent secretory proteins just after these sequences emerge from the large ribosomal subunit (3). Concomitant with this recognition event, SRP modulates the translation of these proteins by reversibly arresting polypeptide elongation (4). The molecular details of this elongation-arrest reaction are unknown; the question remains how SRP could recognize information in the nascent chain and simultaneously affect reactions involved in elongation, since the nascent chain exit site (19) and the peptidyltransferase center (20) in the ribosome are believed to be physically separated by about 16 nm (19). It is of course possible that the mechanism involves allosteric changes across the ribosome itself. However, it also is conceivable that SRP physically bridges the distance between the two sites, recognizing (binding to) signal sequences with one end and modulating the elongation reaction with the other. Arrest of elongation could be effected by blocking the aminoacyl-tRNA binding site or by interfering directly with peptidyltransferase. With further effort, combining high-resolution imaging techniques with the recently produced antibodies against specific polypeptides of SRP, these questions can be addressed directly.

We wish to thank Elizabeth Macpherson for technical assistance in preparing the specimen supports and the Dunlap Observatory for use of the microdensitometer. This work was supported by grants from the National Cancer Institute of Canada, the Medical Research Council of Canada, and the Ontario Cancer Treatment and Research Foundation, and by National Institutes of Health Grant GM32384. P.W. is a recipient of support from the Chicago Community Trust/Searle Scholars Program. D.W.A. is recipient of the Mary Beatty Scholarship.

1. Walter, P. & Blobel, G. (1980) *Proc. Natl. Acad. Sci. USA* **77,** 7112–7116.
2. Walter, P. & Blobel, G. (1982) *Nature (London)* **299,** 691–698.
3. Walter, P., Ibrahimi, I. & Blobel, G. (1981) *J. Cell Biol.* **91,** 545–550.
4. Walter, P. & Blobel, G. (1981) *J. Cell Biol.* **91,** 557–561.
5. Gilmore, R., Blobel, G. & Walter, P. (1982) *J. Cell Biol.* **95,** 463–469.
6. Meyer, D. I., Krause, E. & Dobberstein, B. (1982) *Nature (London)* **297,** 647–650.
7. Walter, P., Gilmore, R. & Blobel, G. (1984) *Cell* **38,** 5–8.
8. Walter, P. & Blobel, G. (1983) *Methods Enzymol.* **96,** 84–93.
9. Walter, P. & Blobel, G. (1983) *Methods Enzymol.* **96,** 682–691.
10. Whiting, R. F. & Ottensmeyer, F. P. (1972) *J. Mol. Biol.* **67,** 173–181.
11. Wall, J., Hainfeld, J., Haschemeyer, R. H. & Mosesson, M. W. (1983) *Ann. N. Y. Acad. Sci.* **408,** 164–179.
12. Andrews, D. W. & Ottensmeyer, F. P. (1982) *Ultramicroscopy* **9,** 337–348.
13. Ottensmeyer, F. P., Whiting, R. F., Schmidt, E. E. & Clemens, J. (1975) *J. Ultrastruct. Res.* **52,** 193–201.
14. Ottensmeyer, F. P., Bazett-Jones, D. P., Hewitt, J. & Price, G. B. (1978) *Ultramicroscopy* **3,** 303–313.
15. Bazett-Jones, D. P. & Ottensmeyer, F. P. (1979) *J. Ultrastruct. Res.* **67,** 255–266.
16. Schultze, H. E. & Heremans, J. F. (1966) in *Molecular Biology of Human Proteins with Special Reference to Plasma Proteins,* (Elsevier, Amsterdam) Vol. 1, p. 150.
17. Boedtker, H. (1968) *Methods Enzymol.* **12,** 429–458.
18. Brackenhoff, G. K. (1974) in *Principles and Techniques of Electron Microscopy,* ed. Hayat, M. A. (Van Nostrand-Reinhold, New York) Vol. 4, pp. 16–42.
19. Bernabeau, C., Tobin, E. M., Fowler, A., Zabin, I. & Lake, J. A. (1983) *J. Cell Biol.* **96,** 1471–1474.
20. Lake, J. A. & Strycharz, W. A. (1981) *J. Mol. Biol.* **153,** 979–992.